Desalination and Water Treatment
www.deswater.com
doi: 10.5004/dwt.2023.29817

304 (2023) 247–256
August

Efficient removal of Congo red by adsorption assisted by heterogeneous Fenton-like degradation using MgAl-CO_3 in neutral pH

Hicham Atout, Zoubir Manaa*, Derradji Chebli, Abdellah Bouguettoucha, Badreddine Meziani

Département de Génie des Procédés, Laboratoire de Génie des Procédés Chimiques, Faculté de Technologie, Université Ferhat Abbas, Sétif-1, 19000 Sétif, Algeria, emails: zoubirmanaa@gmail.com (Z. Manaa), attoutishak@gmail.com (H. Atout), derradji_chebli@yahoo.fr (D. Chebli), bouguettoucha@gmail.com(A. Bouguettoucha), badreddinemeziani25@gmail.com (B. Meziani)

Received 20 February 2023; Accepted 23 July 2023

ABSTRACT

Layered double hydroxides MgAl-CO_3 synthesized by co-precipitation have been used to adsorb and degrade Congo red in aqueous solution. Prepared sample was characterized by scanning electron microscope, Fourier-transform infrared spectra, Brunauer–Emmett–Teller and point of zero charge. The adsorption system provided a value of 22.5 mg/g at natural pH (6.8). The kinetics analysis and isotherms outcomes showed that the adsorption achieve equilibrium adsorption/desorption after 90 min. Which validates that pseudo-second-order is the most accurate fit model. Freundlich isotherm model describes the adsorption isotherms system with R^2 = 0.98. While the photocatalytic degradation proved that the optimal elimination of Congo red was observed by adding H_2O_2 under UV light. The H_2O_2 added under UV light acts as the generator of $OH^{\bullet}$. The dissolved Fe^{3+} reacts with H_2O_2 to form a homogeneous Fenton like by producing $OH^{\bullet}$. The observed degradation decrease after adding Fe^{3+} is explained by the appearance of sludge during the reaction. The Influencing factors of the removal of Congo red have been tested by varying initial pH and H_2O_2 concentrations. The highest degradation was at natural pH (6.8) with C/C_0 = 0.329. While the H_2O_2 concentration exhibits strong degradation with an amount of 3.3 mmol.

Keywords: MgAl-CO_3; Photocatalytic activity; Co-precipitation; Adsorption

1. Introduction

Since synthetic dyes are widely employed in many industrial processes such as textile, cosmetics, and other consumptions [1–4]. The most common dyes frequently found in the textile industry are azo with azo (–N=N–), –SO_3H, and hydroxyl OH, in which showed recalcitrant properties and difficult to eliminate them by classical process due to the production of secondary pollutants [5]. The side effects of the usage cause serious problem for human health even at low concentration [6–10]. Besides this, dyes are known as toxic substances, harmful effects, skin irritation, and mutations. In addition, the dyes contain aromatic cycle causing toxicity and high hazard towards aquatic ecosystems [11–13].

To remove these dyes, different methods were used recently such as adsorption, membrane separation, photochemical degradation, and adsorption [14]. Among these technics, adsorption and advanced oxidation process; due to the low-cost, simplicity, and high efficiency [15]. In this sense, using only adsorption and biological degradation is not sufficient to remove these dyes from wastewater [16]. However, the physical adsorption process that includes the transfer of the pollutant to the solid surface is considered less expensive and easily operated [17].

* Corresponding author.

Nowadays, advanced oxidation processes are an important technology methods for water treatment [18–24]. The iron and hydrogen peroxide have been widely treated as homogeneous Fenton over several years ago [16,25]. Regardless, of the simplicity and the effectiveness of lattice process, various problems are associated to it such as, strict acidic pH, considerable amount of ferric hydroxide, highly expensive H_2O_2 and Fe salts [26–29]. Homogeneous and photo-Fenton like at natural pH is good alternative to overcome these shortfalls of conventional homogeneous Fenton processes. Moreover, many researcher have been using homogeneous Fenton process at acidic conditions [30–34].

In addition, the Fenton like reaction is as follow [35–37]:

$$Fe^{3+} + H_2O_2 \rightarrow Fe^{2+} + H^+ + HO_2^{\bullet} \quad \text{(I)}$$

$$Fe^{2+} + H_2O_2 \rightarrow Fe^{3+} + OH^{\bullet} + OH^- \quad \text{(II)}$$

Layered double hydroxide (LDH) are inorganic and promising materials due to their low cost, easy preparation, high performance and layered structure [38–40]. In addition, it is known as hydrotalcite-type or anionic clays with two dimensional materials containing different elements in single structure. Many of scientific researchers have made LDH as the main target for their scientific experiments due to the presence of: di, trivalent, and anions intercalated in layered, given the possibility to retain different element. Layered double hydroxides is a material formed by divalent and trivalent metal cation hydroxide layers [39–42]. The common case of di and trivalent cations is given by the general chemical formula $[M^{2+}_{1-x}M^{3+}_{x}(OH)_2]^{x+}(A^{n-})_{x/n}\cdot yH_2O$ where M^{2+}(Mg^{2+}, Co^{2+}, Cu^{2+}, Zn^{2+}, etc) and M^{3+}(Al^{3+}, Fe^{3+}, Cr^{3+}, etc) are divalent and trivalent cations, x is $M^{3+}/(M^{2+} + M^{3+})$ and A refers to the interlayer anions (CO_3^{2-}, NO_3^-, Cl^-, SO_4^{2-}, etc) [40,41]. Layered double hydroxides have been widely studied as adsorbents for the removal of micropollutants due to their simple intercalation and modification techniques [43]. LDHs have been used for the adsorption of anionic dyes [44], pharmaceutical compound [45], heavy metals [46] and other pollutants. Synergically, the effectiveness of adsorption and photocatalytic degradation have been widely examined, Atout et al. [16] have provided TiO_2 on the activated carbon to remove methylene blue.

This paper mainly highlighted the preparation of low-cost MgAl-CO_3 by co-precipitation method and calcined at 500°C. This material was selected to overcome the inconvenience caused by acidic pH. The MgAl-CO_3 prepared was used for studying the performance of adsorption and photocatalytic degradation by adding hydrogen peroxide at natural pH. The mechanism of the removal of Congo red was determined by scanning electron microscope (SEM), Fourier-transform infrared spectroscopy (FTIR), Brunauer–Emmett–Teller (BET), and point of zero charge (PZC). Then, the photocatalytic degradation confirms that the degradation is high at naturel pH to exploit the MgO formed after calcination. However, most of the previous studies usually use acidic pH to improve the photocatalytic degradation. Finally, this paper provides low cost LDH for high photocatalytic degradation and adsorption at natural pH.

2. Chemicals and methods

Sodium hydroxide (NaOH, 96%, Sigma-Aldrich, Germany), sodium carbonate (Na_2CO_3, 99.8%), aluminum chloride ($AlCl_3\cdot 9H_2O$, 96%), magnesium chloride ($MgCl_2\cdot 9H_2O$, 98%), hydrochloric acid (HCl, 36%–38%), ferric chloride ($FeCl_3\cdot 6H_2O$, 98%, Sigma-Aldrich, Germany), hydrogen peroxide (H_2O_2, 30%). Congo red was used as the target pollutant.

2.1. Preparation of MgAl-CO_3

Layered double hydroxides (MgAl-CO_3) prepared by co-precipitation method. This method requires the preparation of two solutions, the first one includes divalent and trivalent salts $MgCl_2\cdot 6H_2O$ and $AlCl_3\cdot 9H_2O$. The second solution contains NaOH and Na_2CO_3 in order to intercalate LDH layers by the two anions CO_3^{2-} and OH^-. The preparation was carried out in basic medium to have the precipitation of the metal hydroxides of MgO and $Al(OH)_3$ with ratio of M^{2+}/M^{3+} = 1 in order to have good crystallization of LDH. The synthesis was as following: in two separated beakers of 400 mL, a solution of $MgCl_2\cdot 6H_2O$ and $AlCl_3\cdot 9H_2O$ were mixed with 0.33 mol for each salt. The second solution contains 2 moles of NaOH and 1 mole of Na_2CO_3. Then the two mixtures were added dropwise at pH = 10 for 4 h to form the layered double hydroxides under vigorous stirring in order to ensure the crystallization of the precipitate. The mixture kept stirring in water bath at 60°C for 24 h. Finally, the resulting product was washed several times with distilled water to remove the ions of sodium and chloride and then dried at 60° for 24 h. The dried solid was calcined at 500°C under air for 5 h.

2.2. Characterization

The morphology of MgAl-CO_3 was achieved by SEM (NeoScope JCM-5000, Japan). The crystallographic phases were obtained by X-ray diffraction with a Siemens D5000 Diffractometer with Bragg-Brentano (BB) Geometry and vertical 2-Theta goniometer at 80 kV using CuKα radiation. FTIR spectra were analyzed on a WQ500 spectrophotometer (Marque, Algeria) in the range of 4,500–600 cm^{-1}).

The adsorption/desorption analysis was performed using Micromeritics' Gemini VII (USA) surface area and porosity. The sample was analyzed at –196°C. Prior to analysis, the MgAl-CO_3 sample was degassed in vacuum at 120°C for 24 h. The calculation of specific surface area was performed by BET at P/P_0 = 0.05–0.35.

The point of zero charge was obtained by pH drift method. A different pH (2–12) adjusted by HCl (0.1 mol) or NaOH (0.1 mol) for each point using 25 mg of MgAl-CO_3 and 25 mL of distilled water. Then, the suspension were kept under stirring for 24 h in order to measure the final pH, and plotted vs. initial pH. The point of zero charge was obtained by the value of $pH_{initial} = pH_{final}$.

2.3. Adsorption and photocatalysis measurement

The adsorption experiments were performed using batch method. First, a solution of Congo red was prepared and added in 50 mL of conical beakers with 25 mL dye solutions

and concentration of 25 mg/L of Congo red and mass solid of 25 mg. A given contact time was chosen 0–180 min at room temperature. 4 mL of suspension was centrifuged and analyzed with UV-Visible spectrophotometer at 498 nm. The adsorption capacity was calculated by Eq. (1) [47]:

$$Q = \frac{\left(C_0 - C\right)V}{m} \tag{1}$$

where C_0 and C are the initial and final concentration of Congo red. V and m are volume of the solution and mass of the solid, respectively.

Then, the kinetic adsorption was determined by choosing three different concentrations of Congo red – 12.5, 25, and 50 mg/L. All the experiments were carried out as follows: 25 mL of dye solution and 25 mg of solid were mixed together for each concentration at given interval times. The kinetic adsorption was calculated using Eq. (2) [16]:

$$Q_t = \frac{\left(C_0 - C_t\right)V}{m} \tag{2}$$

where Q_t and C_t are the adsorption capacity and concentration of the solution at any time t. Each test of adsorption was repeated at least twice.

Kinetic models were carried out by using the pseudo-first-order and the pseudo-second-order. The pseudo-first-order is reported in Eq. (3) [48]:

$$\ln\left(Q_e - Q_t\right) = \ln Q_e - k_1 t \tag{3}$$

where Q_e and Q_t are respectively adsorption capacity at equilibrium (mg/g) and at time t (mg/g), k_1 is the rate constant of pseudo-first-order equation (1/h). However, the pseudo-second-order model equation is given by Niu et al. [49]:

$$\frac{t}{Q_t} = \frac{1}{k_2 \cdot Q_e^2} + \frac{1}{Q_e}t \tag{4}$$

where k_2 is the rate constant of pseudo-second-order (g/mg·min).

Transport of Congo red through a boundary layer and from surface into pores of MgAl-CO_3 are measured by intraparticle diffusion model [50]. Moreover, the intraparticle diffusion is the rate-determining factor according to Weber and Morris. Where, the CR adsorption were varied with the square root of time $t^{1/2}$. K_d is the coefficient of intraparticle diffusion (mg/g·min$^{1/2}$), and C is thickness layer diffusion (mg/g).

In addition, the adsorption isotherms explain the interaction between adsorbent and adsorbate in equilibrium adsorption. The adsorption equilibrium was determined at constant temperature by varying initial concentration of Congo red from 10 to 200 mg/L with V = 25 mL of volume and m = 25 mg of mass of adsorbent.

In this sense, Langmuir and Freundlich isotherms were used as two models, which frequently found in the literature at a constant temperature. The adsorption capacity equilibrium conditions is given by He et al. [51]:

$$Q_e = \frac{\left(C_0 - C_e\right)V}{m} \tag{5}$$

where C_e is the concentration of the solution at equilibrium.

Langmuir and Freundlich isotherms are the most frequently models used in the literature describing the linear fit between the adsorbent and adsorbate. The Langmuir isotherm is based on the existing of monolayer on the surface and all sorption sites are identical. This model is given by:

$$Q_e = \frac{Q_m K_L C_e}{1 + K_L C_e} \tag{6}$$

where K_L is the Langmuir constant (L/mg) and Q_m is the maximum capacity (mg/g). The linear transformed equation is written as follows:

$$\frac{C_e}{Q_e} = \frac{C_e}{Q_m} + \frac{1}{K_L \cdot Q_m} \tag{7}$$

The Freundlich isotherm is the exponential distribution of active centers and characteristic of heterogeneous surfaces and assumes heterogeneous sites energies with unlimited levels of sorption. The equation of Freundlich is given by:

$$Q_e = K_F \left(C_e\right)^{1/n} \tag{8}$$

where K_F and $1/n$ are respectively constant of Freundlich and sorption intensity.

The linear transformed equation is written as follows:

$$\ln Q_e = \ln K_F + \frac{1}{n}\ln C_e \tag{9}$$

The experimental data were also analyzed by Dubinin–Radushkevich model in which is described by Mate and Mishra [52]:

$$q_e = q_m e^{-K_{D-R}\varepsilon^2} \tag{10}$$

The linear transformed equation is written by:

$$\ln q_e = \ln q_m - K_{D-R}\varepsilon^2 \tag{11}$$

where K is the constant of the adsorption energy (mol^2/J^2) and ε is the adsorption potential given by Polanyi's formula [53], where T is the temperature (K) and R is the ideal gas constant (8.314 J/mol·K).

$$\varepsilon = RT\ln\left(1 + \frac{1}{C_e}\right) \tag{12}$$

Homogeneous photo-Fenton like were performed as follows: a volume of 100 mL Congo red, with initial concentration of 25 mg/L and at natural pH was added into a cylindrical shape reactor of 100 mL in front of an ultraviolet lamp worked at 24 W with 365 nm of wavelength. The

distance between the lamp and the reactor is 15 mm. Congo red was used as a model of pollutant in this study due to its presence in wastewaters [54]. Then, 100 mg of MgAl-CO_3 were dispersed in 50 mL of Congo red solution. The suspension was stirred in the dark conditions to ensure the adsorption/desorption equilibrium. After 90 min, a certain amount of peroxide hydrogen was added to the mixture in order to ensure the mineralization of Congo red. To complete the reaction of photo-Fenton like, 0.001 mol of Fe^{3+} were added to the solution. At given time intervals, the concentrations of Congo red were centrifuged and analyzed using UV-Visible spectrophotometer (Shimadzu UV-1700, Japan) by determining the absorbance at 498 nm.

2.4. Performance evaluation for operating parameters

The effect of initial pH plays a key role in the reaction of heterogeneous photo-Fenton like. The experiments were carried out under UV light at different pH from 4 to 12. To vary the initial pH, HCl and NaOH were used for acid and basic aqueous solution, respectively. The other experimental conditions were as the following: V = 50 mL, m = 100 mg and C_0 = 25 mg/L.

Since the H_2O_2 is a source of hydroxyl radicals, in which can play an important effect in catalytic degradation. First, a predetermined quantity of H_2O_2 was added to 100 mL of 25 mg/L of Congo red solution, as the following reaction:

$$C_{32}H_{22}N_6Na_2O_6S_2 + 91H_2O \rightarrow 32CO_2 + 98H_2O + 4HNO_3 + 2H_2SO_4 + 2NaNO_3 \quad \text{(III)}$$

The pH solution was kept at natural value 6.8. Secondly, the photocatalytic degradation was performed by turning on the UV light. Different concentration of H_2O_2 were used as: 2, 3.3, 4 and 7 mmol/L, and 3 mL of suspension was withdrawn at different interval time and filtered through centrifugation to further analyze it by UV-Visible.

3. Results and discussion

3.1. Characterization

The SEM images of MgAl-CO_3 are shown in Fig. 1, where the surface of MgAl-CO_3 is rigorous in high and low magnifications. In addition, micro-sized agglomerations are observed by higher contrasts and the particles are irregular in shape. Moreover, comparable results found by Wang et al. [55] using double lamellar hydroxides MgAlFe for methylene blue adsorption.

Fig. 2 presents X-ray diffraction of as prepared MgAl-CO_3. The sample reveals peaks that can assigned to the 2θ angle 23.4°, 34.8°, 39.5°, 45.5°, 60.8° and 62.3° corresponding to planes of 006°, 012°, 015°, 200°, 110° and 113°. It is clear that the peak of MgO is clear at 45.5° which can play the role of semiconductor during the degradation of Congo red.

Fig. 3 shows the results of FTIR. The MgAl-CO_3 material was measured over a wavelength range of 4500–600 cm^{-1}. Two characteristic bands are observed around 3670 and 3400 cm^{-1} correspond respectively to the elongation bonds of carbonate ions and to hydroxyl groups –OH. The absorption bands around 2980 and 2910 cm^{-1} are related to the elongations of inter-lamellar carbonates. The band of 1620 cm^{-1} is attributed to the OH bending vibration of water [7]. The 1380 cm^{-1} band exhibits the asymmetric stretching vibration of C–O [7]. The bands smaller than 1000 cm^{-1} correspond to the M–OH and O–M–O bonds with M = Mg, Al [55].

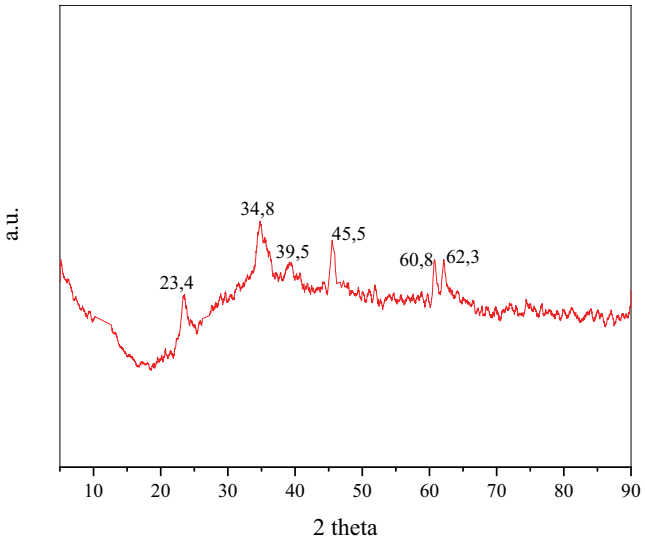

Fig. 2. X-ray diffraction of MgAl-CO_3.

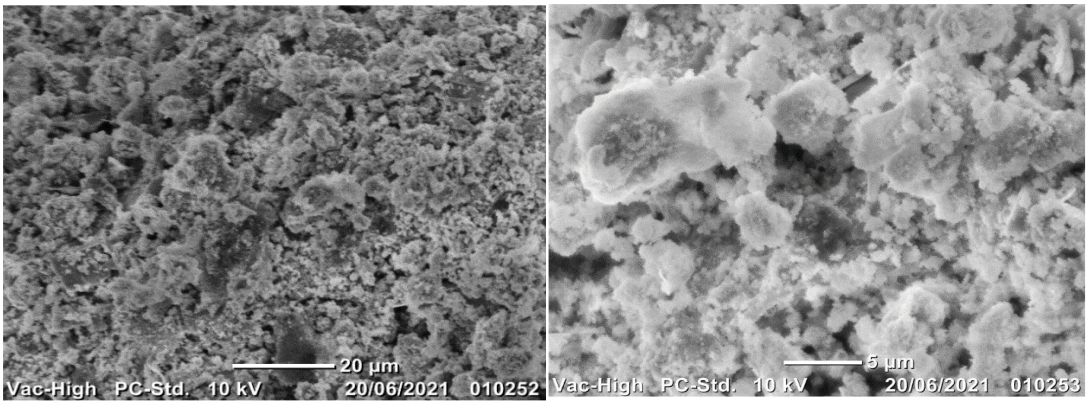

Fig. 1. Scanning electron microscope at high and low magnification of MgAl-CO_3.

The specific surface area of MgAl-CO_3 is 41.90 m^2/g. During the calcination, water and carbon dioxide were removed to favorite the adsorption of Congo red and facilitate the photocatalytic degradation due to the near molecules of pollutant [16].

The point of zero charge of MgAl-CO_3 is around 8.81 (Fig. 4). This lattice value indicates that the high adsorption would be below 8.81, in which in agreement with the results of pH effect. In addition, for Congo red adsorption at pH > pH_{PZC} the electrostatic attraction is between the positively charged MgAl-CO_3 and negatively charged Congo red [56]. Whereas, electrostatic repulsion was between the negatively charged MgAl-CO_3 and positively charged Congo red. The highest photocatalytic degradation was clear at pH = 6.8 with C/C_0 = 0.329 as observed in Fig. 10.

5.2. Adsorption and photocatalysis

The adsorption test of Congo red was performed using function of time to determine the adsorption capacity. This step is important to find the maximum adsorption where adsorption–desorption equilibrium time is known. According to Fig. 5, the MgAl-CO_3 material exhibits a great adsorption of Congo red due to the negative charge of the dye by facilitating ion exchange between this dye and the ions of the inter-lamellar space. Furthermore, for concentrations 10, 25 and 50 mg/L, the adsorption is very fast from the first minutes and the equilibrium is reached after 90 min and the adsorption capacity reaches respectively 8, 22 and 45 mg/g. In this case, increasing concentration suggests an increase in adsorption capacity.

Additionally, it is clear that the equilibrium time for this material is estimated to be approximately 90 min. After that interval of time, there is an adsorption–desorption equilibrium between the adsorbent and the adsorbate.

Fig. 6a and b show pseudo-first-order and pseudo-second-order [48,49].

The low correlation of adsorption capacity of pseudo-first-order is clear with R^2 = 0.24, 0.86, and 0.8 for each initial concentration 10, 25 and 50 mg/L, respectively. This confirms that the pseudo-first-order model is not suitable for the description of the adsorption kinetics of the experimental results. However, the pseudo-second-order model shows better results with R^2 = 0.766, 0.186 and 0.888 for 10, 25 and 50 mg/L, respectively. In this case, the optimal fit model is pseudo-second-order that describes our experimental data.

The intraparticle diffusion curve showed two linear parts attributed respectively to the diffusion in macropores diffusion between Congo red and MgAl-CO_3 (Fig. 6c). While the second-step was attributed micropores. In addition, the results present that the curve Q_t vs. $f(t^{1/2})$ do not across the origin and consequently the intraparticle diffusion is not the limiting step [14]. This means that the boundary layer diffusion and the intraparticle diffusion are involved in the adsorption.

The isotherm spectra of MgAl-CO_3 shows that when the equilibrium concentration of Congo red increases (Fig. 7a), the adsorption capacity increases to reach saturation of all sites on the surface of the adsorbents. The isotherm exhibits similarities to the L-type according to the Gill classification,

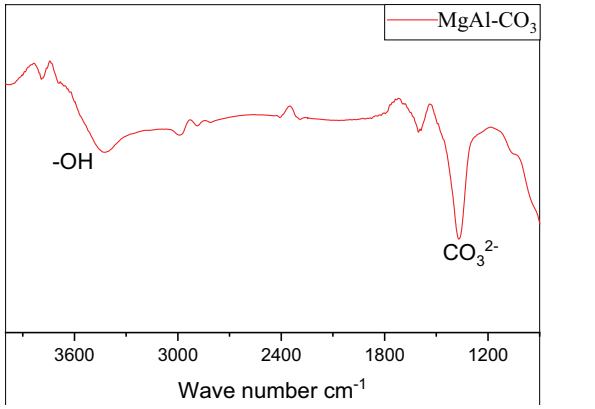

Fig. 3. Fourier-transform infrared spectra of MgAl-CO_3.

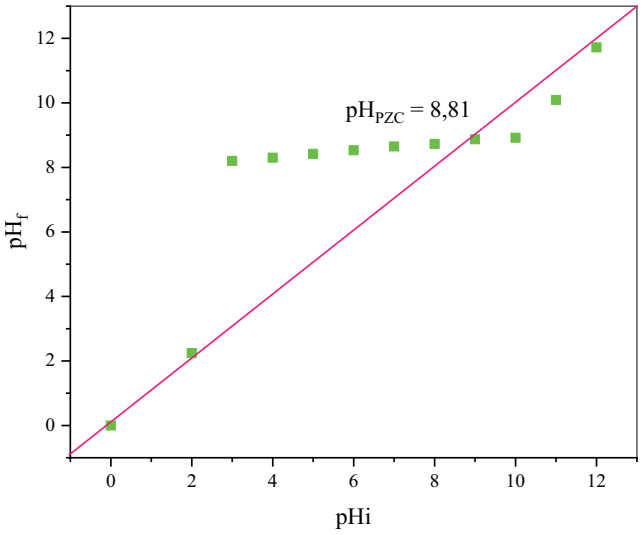

Fig. 4. Final pH as a function of initial pH to determine the point of zero charge.

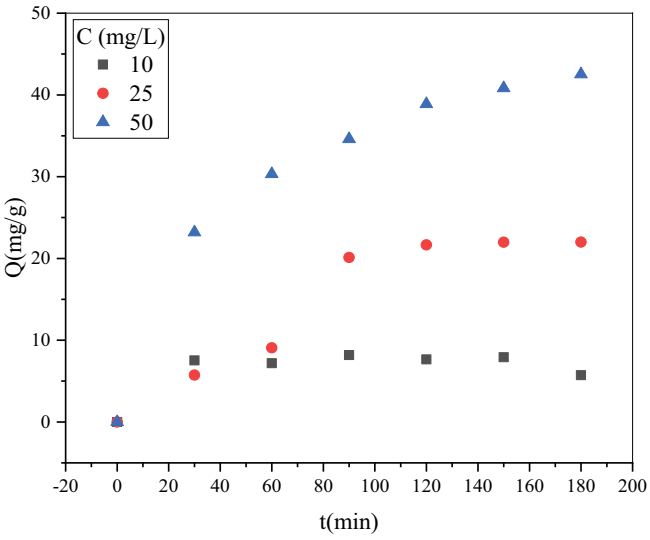

Fig. 5. Adsorption kinetics of MgAl-CO_3.

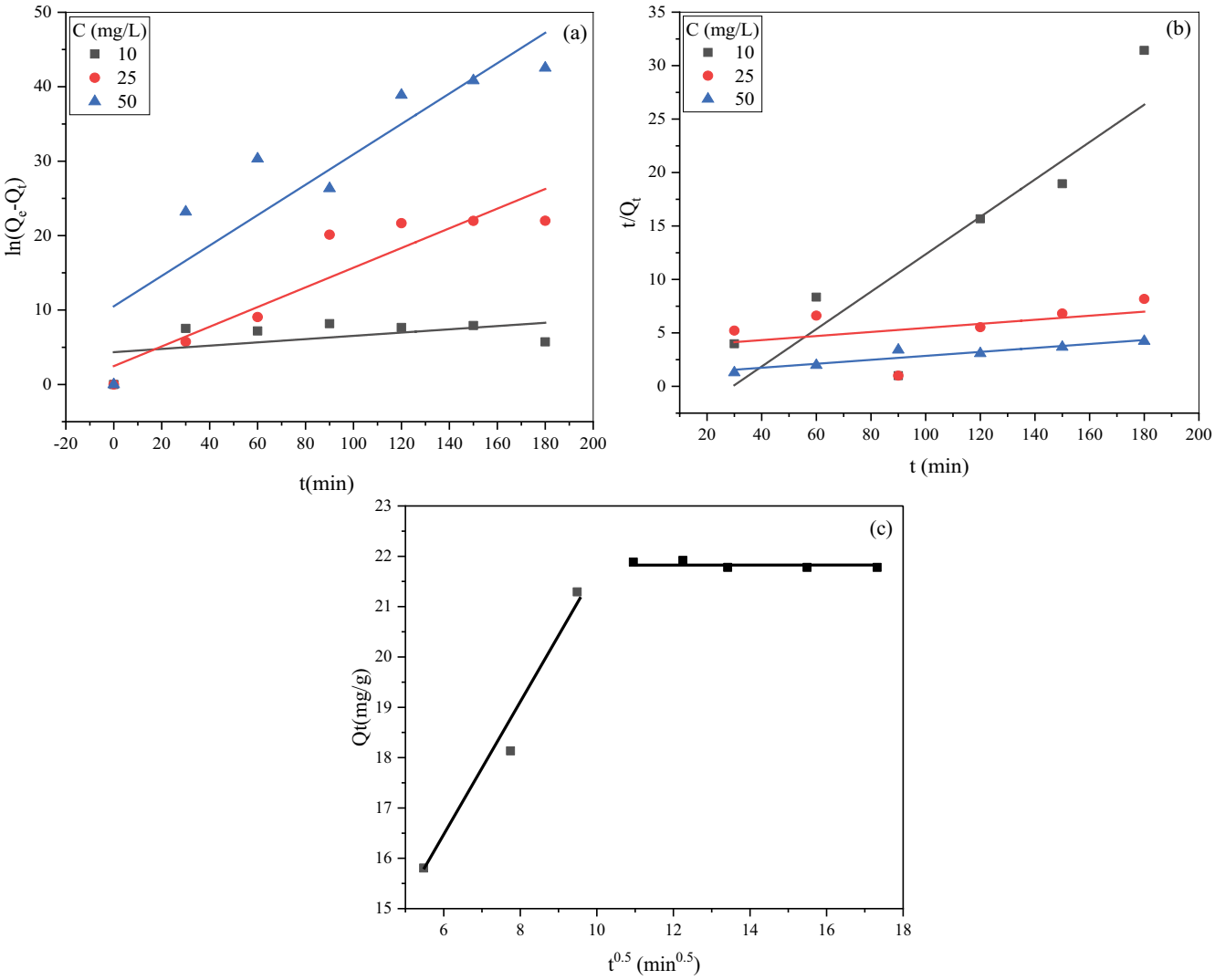

Fig. 6. Kinetic modeling of pseudo-first-order (a), pseudo-second-order (b), and intraparticle diffusion (c).

which means a concavity turned downwards which indicates a decrease in free sites as the adsorption progresses and indicates. This phenomenon occurs when the forces of attraction between the adsorbed molecules are weak. It is often observed when molecules are adsorbed flat, that their lateral attraction is minimized. It can also appear when the molecules are adsorbed vertically and when the adsorption competition between the solvent and the solute is weak.

The modeling of adsorption isotherms were performed to understand the mechanism of adsorption, in which displayed for Congo red adsorption onto MgAl-CO_3. The plots and the fitting model using determined efficiency R^2 for the Langmuir and Freundlich models (Fig. 7b and c). It is clear that the isotherm followed the Freundlich model, with the highest value R^2 = 0.995, followed by the Langmuir model, R^2 = 0.952 (Table 1). The Freundlich isotherm defines the surface heterogeneity and the exponential distribution of active sites and their energies.

The value of adsorption energy was calculated using linear Dubinin–Radushkevich isotherm shown in Fig. 7d, with $E = 1/(2K_{D\text{-}R})^{0.5}$ in which confirms that the mechanism of the adsorption is physisorption with E = 0.00378 J/mol.

Fig. 8a shows the reactions of degradation type (MgAl-CO_3/H_2O_2/UV) at natural pH. Indeed, the photolysis reaction has no catalytic efficiency. While, after adding H_2O_2 with the MgAl-CO_3 catalyst in the dark, Congo red was degraded with C/C_0 = 0.458 (R = 54.2%). Significant degradation was observed when using UV light at natural pH, this degradation up to C/C_0 = 0.329 (R = 67.1%). This degradation is mainly due to the decomposition of H_2O_2 by ultraviolet irradiation [57], on the other hand it could be due to the formation of MgO during calcination. In this case, the latter compound plays a role of the semiconductor. Finally, for the reaction of photo-Fenton like by adding Fe^{3+} (liquid iron) according to reactions (IV)–(IX) [18,21,23]. This catalytic degradation is less efficient than the previous one (with C/C_0 = 0.407 with efficient of 59.3%). Usually, this disadvantage can be related to the appearance of sludge during the reaction, this sludge will prevent the Fenton reaction. Even at acidic pH (pH = 3) the formation of sludge is still laid.

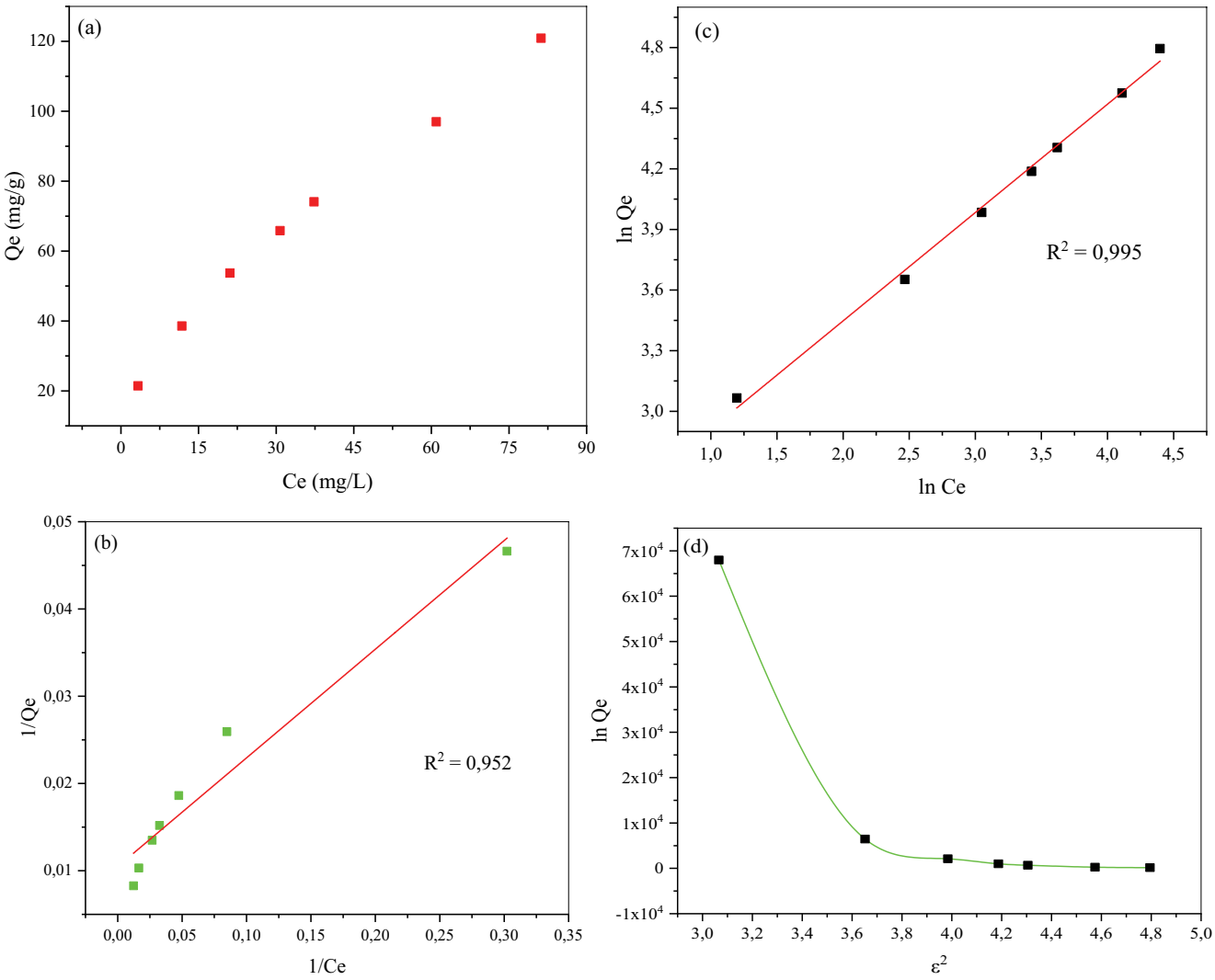

Fig. 7. Adsorption isotherm of MgAl-CO_3 (a), Langmuir isotherm, (b) Freundlich isotherm (c), and Dubinin–Radushkevich model (d).

Table 1
Isotherm constants and correlation coefficients of MgAl-CO_3

Sample	Langmuir			Freundlich			Dubinin–Radushkevich		
	K_L	Q_m (mg/g)	R^2	K_F	n	R^2	Q_m (mg/g)	E	R^2
MgAl-CO_3	6.44	8.06	0.95	6.44	1.88	0.99	11.95	0.00378	0.662

$$Fe^{3+} + H_2O_2 \rightarrow Fe^{2+} + H^+ + HO_2^{\bullet} \quad \text{(IV)}$$

$$Fe^{3+} + H_2O \rightarrow Fe^{2+} + OH^{\bullet} + H^+ \quad \text{(V)}$$

$$H_2O_2 + UV \rightarrow OH^{\bullet} + OH^{\bullet} \quad \text{(VI)}$$

$$Fe^{3+} + HO_2^{\bullet} \rightarrow Fe^{2+} + O_2 + H^+ \quad \text{(VII)}$$

$$H_2O_2 + OH^{\bullet} \rightarrow H_2O + HO_2^{\bullet} \quad \text{(VIII)}$$

$$OH^{\bullet} + \text{Congo Red } H_2O + CO_2 + \text{Mineral products} \quad \text{(IX)}$$

The kinetics of degradation by different reactions were performed using the first-order model described in the following equation: $\ln C/C_0 = k_{app}t$ (Fig. 9) where k_{app} is the apparent rate constant of the first-order reaction (min^{-1}), C_0 is the initial concentration and C is the meaning concentration at a given time. As shown in Table 2, the apparent constant of photocatalytic activity of Congo red were determined from the k_{app} in which was higher in the case of MgAl-CO_3/H_2O_2/UV compared to the degradation with k_{app} = 0.0028 min^{-1}.

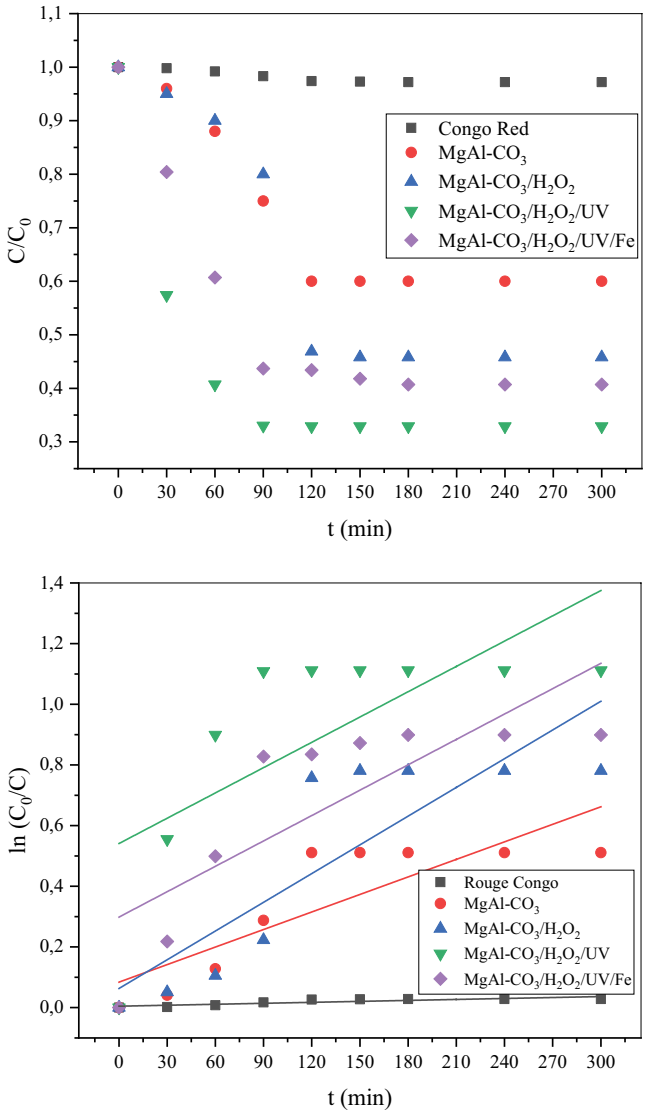

Fig. 8. Photocatalytic degradation efficiency of Congo red under UV light (a) and variation of ln(C_0/C) vs. irradiation time (b).

However, the k_{app} of MgAl-CO_3/H_2O_2 has a value of 0.00216 min^{-1}.

3.3. Performance evaluation for operating parameters

The effect of initial pH on Congo red degradation is depicted in Fig. 9. The photocatalytic degradation was recorded with pH acid, natural and basic. It can be seen that the highest degradation is at natural pH with C/C_0 = 0.329. However, at acidic and basic mediums, lower degradation observed and reaches C/C_0 = 0.355 and 0.410, respectively.

Fig. 10 shows the effect of H_2O_2 on the degradation of Congo red by MgAl-CO_3. When the peroxide hydrogen was increased from 3.3 to 7 mmol/L, the degradation efficiency decreased from C/C_0 = 0.329–0.470. The higher concentration of hydroxyl radicals (–OH•) in the solution exhibits scavenging of OH• by the excess of H_2O_2 in which generates les reactive species such as HOO• [57].

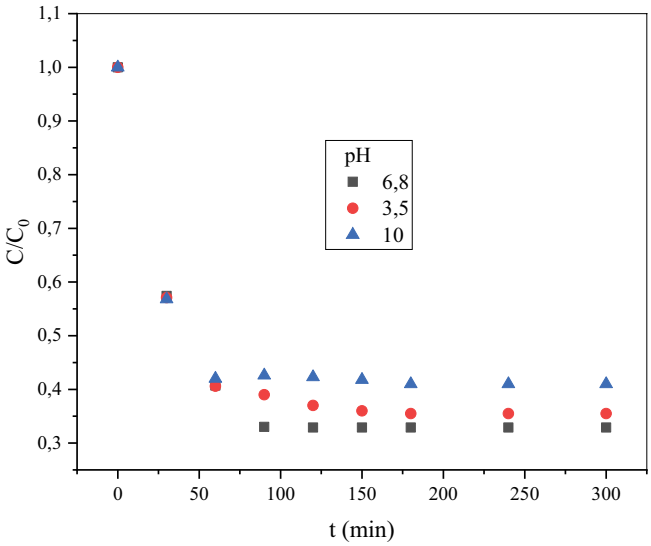

Fig. 9. Effect of initial pH on the photocatalytic degradation after equilibrium time for the reaction of MgAl-CO_3/H_2O_2/UV.

Table 2
Apparent first-order rate constants (k_{app}) for the photodegradation of Congo red

Photocatalyst	k_{app} (min^{-1})·10^{-3}
Congo red	1.06
MgAl-CO_3	1.93
MgAl-CO_3/H_2O_2	2.16
MgAl-CO_3/H_2O_2/UV	2.80
MgAl-CO_3/UV/Fe	2.77

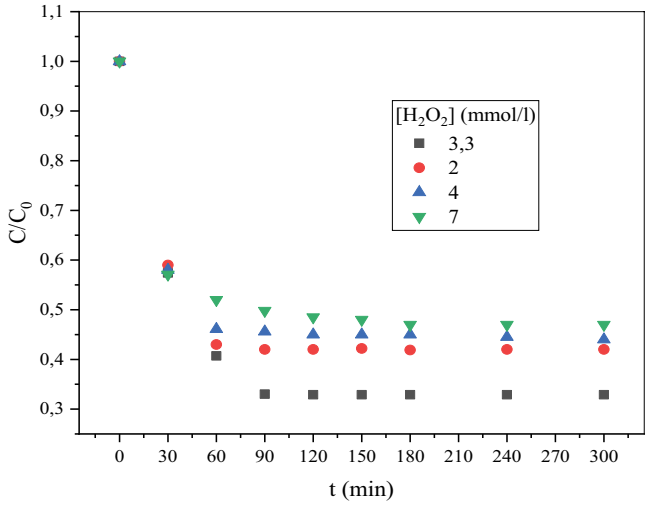

Fig. 10. Initial concentration of H_2O_2 using the reaction of MgAl-CO_3/H_2O_2/UV.

4. Conclusion

The LDH prepared by co-precipitation method was used for adsorption and photocatalytic degradation. In this

work, we proved that MgAl-CO_3 presented an adsorption of 22.5 mg/g, this adsorption is due to the surface area of MgAl-CO_3. The physico-chemical characterizations revealed the SEM images of LDH in which were rigorous in high and low magnification. The point of zero charge is around 8.81, that means Congo red might have a good adsorption and degradation.

The kinetic adsorption results showed that adsorption was very fast even with high concentration and the equilibrium time was estimated to approximately 90 min for the initial concentration of 25 mg/L. Then the kinetic modeling system confirmed that the pseudo-second-order was suitable for this adsorption and describes our experimental data. In addition, the isotherm modeling results presented that Langmuir model was the most accurate fit model with $R^2 = 0.982$ compared to the Freundlich model ($R^2 = 0.92$).

Moreover, the photocatalytic degradation gave a significant elimination when using H_2O_2 under UV light and at natural pH, this degradation up to $C/C_0 = 0.329$. The significant results are mainly related to the generating $OH^•$ and also to the formation of MgO during the calcination phase which plays the role of semiconductor. The highest degradation in the case of effect of pH was at natural pH with $C/C_0 = 0.329$. However, at acidic and basic mediums, lower degradation observed and reaches $C/C_0 = 0.355$ and 0.410, respectively. The variation of H_2O_2 allows the higher concentration of hydroxyl radicals (–$OH^•$) in the solution exhibits scavenging of $OH^•$ by the excess of H_2O_2 in which generates less reactive species such as $HOO^•$.

References

[1] J. Li, S. lin Zhou, G.-B. Hong, C.-T. Chang, Hydrothermal preparation of P25–graphene composite with enhanced adsorption and photocatalytic degradation of dyes, Chem. Eng. J., 219 (2013) 486–491.

[2] K. Azam, N. Shezad, I. Shafiq, P. Akhter, F. Akhtar, F. Jamil, S. Shafique, Y.-K. Park, M. Hussain, A review on activated carbon modifications for the treatment of wastewater containing anionic dyes, Chemosphere, 306 (2022) 135566, doi: 10.1016/j.chemosphere.2022.135566.

[3] Y. Xiong, P.J. Strunk, H. Xia, X. Zhu, H.T. Karlsson, Treatment of dye wastewater containing acid orange II using a cell with three-phase three-dimensional electrode, Water Res., 35 (2001) 4226–4230.

[4] G. Abbas Ashraf, M. Hassan, R. Tur Rasool, W. Abbas, L. Zhang, Mesoporous SnMgNd substituted M-hexaferrite catalyzed heterogeneous photo-Fenton-like activity for degradation of methylene blue, J. Colloid Interface Sci., 557 (2019) 408–422.

[5] M. Sillanpää, A.H. Mahvi, D. Balarak, A.D. Khatibi, Adsorption of Acid orange 7 dyes from aqueous solution using polypyrrole/nanosilica composite: experimental and modelling, Int. J. Environ. Anal. Chem., 103 (2020) 212–229.

[6] N. Arora, A. Mehta, A. Mishra, S. Basu, 4-Nitrophenol reduction catalysed by Au-Ag bimetallic nanoparticles supported on LDH: homogeneous vs. heterogeneous catalysis, Appl. Clay Sci., 151 (2018) 1–9.

[7] D. Chebli, A. Bouguettoucha, A. Reffas, C. Tiar, M. Boutahala, H. Gulyas, A. Amrane, Removal of the anionic dye Biebrich scarlet from water by adsorption to calcined and non-calcined Mg–Al layered double hydroxides, Desal. Water Treat., 57 (2016) 22061–22073.

[8] R.G.L. Gonçalves, P.A. Lopes, J.A. Resende, F.G. Pinto, J. Tronto, M.C. Guerreiro, L.C.A. de Oliveira, W. de Castro Nunes, J.L. Neto, Performance of magnetite/layered double hydroxide composite for dye removal via adsorption, Fenton and photo-Fenton processes, Appl. Clay Sci., 179 (2019) 105152, doi: 10.1016/j.clay.2019.105152.

[9] X. Guo, K. Wang, Y. Xu, Tartaric acid enhanced $CuFe_2O_4$-catalyzed heterogeneous photo-Fenton-like degradation of methylene blue, Mater. Sci. Eng., B, 245 (2019) 75–84.

[10] W. Gao, S. Zhang, G. Wang, J. Cui, Y. Lu, X. Rong, C. Gao, A review on mechanism, applications and influencing factors of carbon quantum dots based photocatalysis, Ceram. Int., 48 (2022) 35986–35999.

[11] J. Xiao, J. Lai, R. Li, X. Fang, D. Zhang, P. Tsiakaras, Y. Wang, Enhanced ultrasonic-assisted heterogeneous fenton degradation of organic pollutants over a new copper magnetite (Cu-Fe_3O_4/Cu/C) nanohybrid catalyst, Ind. Eng. Chem. Res., 59 (2020) 12431–12440.

[12] S.D. Shifflett, J. Schubauer-Berigan, Assessing the risk of utilizing tidal coastal wetlands for wastewater management, J. Environ. Manage., 236 (2019) 269–279.

[13] Y.A. Patil, V. Mehta, M. Jachak, R. Bhise, K. Patel, G.S. Shankarling, Facile and rapid synthesis of novel hybrid pigments and their application as colorants in high-performance polymer, J. Mol. Struct., 1273 (2023) 134354, doi: 10.1016/j.molstruc.2022.134354.

[14] J. Xia, Y. Gao, G. Yu, Tetracycline removal from aqueous solution using zirconium-based metal-organic frameworks (Zr-MOFs) with different pore size and topology: adsorption isotherm, kinetic and mechanism studies, J. Colloid Interface Sci., 590 (2021) 495–505.

[15] S. Wang, C. Yuan, F.F. Zafar, M. Wei, F. Marrakchi, B. Cao, Y. Fu, Facile synthesis of *chlorella*-derived autogenous N-doped porous biochar for adsorption on tetracycline, Environ. Pollut., 330 (2023) 121717, doi: 10.1016/j.envpol.2023.121717.

[16] H. Atout, A. Bouguettoucha, D. Chebli, J.M. Gatica, H. Vidal, M.P. Yeste, A. Amrane, Integration of adsorption and photocatalytic degradation of methylene blue using TiO_2 supported on granular activated carbon, Arabian J. Sci. Eng., 42 (2017) 1475–1486.

[17] R.A. Alvarez-Puebla, C. Valenzuela-Calahorro, J.J. Garrido, Theoretical study on fulvic acid structure, conformation and aggregation, Sci. Total Environ., 358 (2006) 243–254.

[18] M.S. Vasilyeva, V.S. Rudnev, A.A. Zvereva, A. Yu. Ustinov, O.D. Arefieva, V.G. Kuryavyi, G.A. Zverev, FeO_x,SiO_2,TiO_2/Ti composites prepared using plasma electrolytic oxidation as photo-Fenton-like catalysts for phenol degradation, J. Photochem. Photobiol., A, 356 (2018) 38–45.

[19] J.-M. Herrmann, C. Guillard, P. Pichat, Heterogeneous photocatalysis : an emerging technology for water treatment, Catal. Today, 17 (1993) 7–20.

[20] B. Palas, G. Ersöz, S. Atalay, Photo-Fenton-like oxidation of tartrazine under visible and UV light irradiation in the presence of $LaCuO_3$ perovskite catalyst, Process Saf. Environ. Prot., 111 (2017) 270–282.

[21] K. Wang, H. Niu, J. Chen, J. Song, C. Mao, S. Zhang, Y. Gao, Immobilizing $LaFeO_3$ nanoparticles on carbon spheres for enhanced heterogeneous photo-Fenton like performance, Appl. Surf. Sci., 404 (2017) 138–145.

[22] M. Hartmann, S. Kullmann, H. Keller, Wastewater treatment with heterogeneous Fenton-type catalysts based on porous materials, J. Mater. Chem., 20 (2010) 9002–9017.

[23] J. Herney-Ramirez, M.A. Vicente, L.M. Madeira, Heterogeneous photo-Fenton oxidation with pillared clay-based catalysts for wastewater treatment: a review, Appl. Catal., B, 98 (2010) 10–26.

[24] C. Han, G. Huang, D. Zhu, K. Hu, Facile synthesis of MoS_2/Fe_3O_4 nanocomposite with excellent Photo-Fenton-like catalytic performance, Mater. Chem. Phys., 200 (2017) 16–22.

[25] X. Han, T. Chen, J. Li, F. Cheng, M. Zhang, M. Guo, Synthesis of (Ni,Mg,Cu)Fe_2O_4 from nickel sulfide ore: a novel heterogeneous photo-Fenton-like catalyst with enhanced activity in the presence of oxalic acid, J. Photochem. Photobiol., A, 390 (2020) 112308, doi: 10.1016/j.jphotochem.2019.112308.

[26] M. Hassan, H. Olvera-Vargas, X. Zhu, B. Zhang, Y. He, Microbial electro-Fenton: an emerging and energy-efficient platform for environmental remediation, J. Power Sources, 424 (2019) 220–244.

[27] S. Su, Y. Liu, X. Liu, W. Jin, Y. Zhao, Transformation pathway and degradation mechanism of methylene blue through β-FeOOH@GO catalyzed photo-Fenton-like system, Chemosphere, 218 (2019) 83–92.
[28] S. Bae, D. Kim, W. Lee, Degradation of diclofenac by pyrite catalyzed Fenton oxidation, Appl. Catal., B, 134–135 (2013) 93–102.
[29] T. Zhang, T. ki Oyama, S. Horikoshi, H. Hidaka, J. Zhao, N. Serpone, Photocatalyzed N-demethylation and degradation of methylene blue in titania dispersions exposed to concentrated sunlight, Sol. Energy Mater. Sol. Cells, 73 (2002) 287–303.
[30] K. Sharma, P. Raizada, A. Hosseini-Bandegharaei, P. Thakur, R. Kumar, V.K. Thakur, V.-H. Nguyen, S. Pardeep, Fabrication of efficient CuO/graphitic carbon nitride based heterogeneous photo-Fenton like catalyst for degradation of 2, 4 dimethyl phenol, Process Saf. Environ. Prot., 142 (2020) 63–75.
[31] D. Lei, J. Xue, X. Peng, S. Li, Q. Bi, C. Tang, L. Zhang, Oxalate enhanced synergistic removal of chromium(VI) and arsenic(III) over $ZnFe_2O_4$/g-C_3N_4: Z-scheme charge transfer pathway and photo-Fenton like reaction, Appl. Catal., B, 282 (2021) 119578, doi: 10.1016/j.apcatb.2020.119578.
[32] H. Yu, G. Liu, R. Jin, J. Zhou, Goethite-humic acid coprecipitate mediated Fenton-like degradation of sulfanilamide: the role of coprecipitated humic acid in accelerating Fe(III)/Fe(II) cycle and degradation efficiency, J. Hazard. Mater., 403 (2021) 124026, doi: 10.1016/j.jhazmat.2020.124026.
[33] X. Chen, R. Zhuan, J. Wang, Assessment of degradation characteristic and mineralization efficiency of norfloxacin by ionizing radiation combined with Fenton-like oxidation, J. Hazard. Mater., 404 (2021) 124172, doi: 10.1016/j.jhazmat.2020.124172.
[34] S. Wu, D. Yang, Y. Zhou, H. Zhou, S. Ai, Y. Yang, Z. Wan, L. Luo, L. Tang, D.C.W. Tsang, Simultaneous degradation of *p*-arsanilic acid and inorganic arsenic removal using M-rGO/PS Fenton-like system under neutral conditions, J. Hazard. Mater., 399 (2020) 123032, doi: 10.1016/j.jhazmat.2020.123032.
[35] M.L.A. Ramalho, V.S. Madeira, I.L.O. Brasileiro, P.C.R. Fernandes, C.B.M. Barbosa, S. Arias, J.G.A. Pacheco, Synthesis of mixed oxide Ti/Fe_2O_3 as solar light-induced photocatalyst for heterogeneous photo-Fenton like process, J. Photochem. Photobiol., A, 404 (2021) 112873, doi: 10.1016/j.jphotochem.2020.112873.
[36] A.A. Oladipo, A.O. Ifebajo, M. Gazi, Magnetic LDH-based CoO–$NiFe_2O_4$ catalyst with enhanced performance and recyclability for efficient decolorization of azo dye via Fenton-like reactions, Appl. Catal., B, 243 (2019) 243–252.
[37] G. Liu, Y. Zhang, H. Yu, R. Jin, J. Zhou, Acceleration of goethite-catalyzed Fenton-like oxidation of ofloxacin by biochar, J. Hazard. Mater., 397 (2020) 122783, doi: 10.1016/j.jhazmat.2020.122783.
[38] S. Li, C.I. Ezugwu, S. Zhang, Y. Xiong, S. Liu, Co-doped MgAl-LDHs nanosheets supported Au nanoparticles for complete catalytic oxidation of HCHO at room temperature, Appl. Surf. Sci., 487 (2019) 260–271.
[39] P. Zhong, Q. Yu, J. Zhao, S. Xu, X. Qiu, J. Chen, Degradation of bisphenol A by Fe-Al layered double hydroxides: a new synergy of homo- and heterogeneous Fenton systems, J. Colloid Interface Sci., 552 (2019) 122–133.
[40] R.G.L. Gonçalves, H.M. Mendes, S.L. Bastos, L.C. D'Agostino, J. Tronto, S.H. Pulcinelli, C.V. Santilli, J.L. Neto, Fenton-like degradation of methylene blue using Mg/Fe and MnMg/Fe layered double hydroxides as reusable catalysts, Appl. Clay Sci., 187 (2020) 105477, doi: 10.1016/j.clay.2020.105477.
[41] H. Wang, M. Jing, Y. Wu, W. Chen, Y. Ran, Effective degradation of phenol via Fenton reaction over CuNiFe layered double hydroxides, J. Hazard. Mater., 353 (2018) 53–61.
[42] J. Bai, Y. Liu, X. Yin, H. Duan, J. Ma, Efficient removal of nitrobenzene by Fenton-like process with Co-Fe layered double hydroxide, Appl. Surf. Sci., 416 (2017) 45–50.
[43] M. Daud, A. Hai, F. Banat, M.B. Wazir, M. Habib, G. Bharath, M.A. Al-Harthi, A review on the recent advances, challenges and future aspect of layered double hydroxides (LDH) – containing hybrids as promising adsorbents for dyes removal, J. Mol. Liq., 288 (2019) 110989, doi: 10.1016/j.molliq.2019.110989.
[44] A.-L. Johnston, E. Lester, O. Williams, R.L. Gomes, Understanding layered double hydroxide properties as sorbent materials for removing organic pollutants from environmental waters, J. Environ. Chem. Eng., 9 (2021) 105197, doi: 10.1016/j.jece.2021.105197.
[45] G. Rathee, N. Singh, R. Chandra, Simultaneous elimination of dyes and antibiotic with a hydrothermally generated NiAlTi layered double hydroxide adsorbent, ACS Omega, 5 (2020) 2368–2377.
[46] Y. Xie, X. Yuan, Z. Wu, G. Zeng, L. Jiang, X. Peng, H. Li, Adsorption behavior and mechanism of Mg/Fe layered double hydroxide with Fe_3O_4-carbon spheres on the removal of Pb(II) and Cu(II), J. Colloid Interface Sci., 536 (2019) 440–455.
[47] N.S. Jamaluddin, N.H. Alias, S. Samitsu, N.H. Othman, J. Jaafar, F. Marpani, W.J. Lau, Y.Z. Tan, Efficient chromium(VI) removal from wastewater by adsorption-assisted photocatalysis using MXene, J. Environ. Chem. Eng., 10 (2022) 108665, doi: 10.1016/j.jece.2022.108665.
[48] T. Song, Q. Luo, F. Gao, B. Zhao, X. Hao, Z. Liu, Adsorption and electro-assisted method removal of boron in aqueous solution by nickel hydroxide, J. Ind. Eng. Chem., 118 (2023) 372–382.
[49] H. Niu, H. Yang, L. Tong, A.R. Kamali, The adsorption characteristics and performance of gold onto elemental carbon extracted from refractory carbonaceous gold concentrate, Colloids Surf., A, 658 (2023) 130635, doi: 10.1016/j.colsurfa.2022.130635.
[50] D.D.A. Buelvas, L.P. Camargo, I.K.I. Salgado, B.L.S. Vicentin, D.F. Valezi, L.H. Dall'Antonia, C.R.T. Tarley, E.D. Mauro, Study and optimization of the adsorption process of methylene blue dye in reusable polyaniline-magnetite composites, Synth. Met., 292 (2023) 117232, doi: 10.1016/j.synthmet.2022.117232.
[51] E. He, N. Liu, Y. Zhou, Z. Wang, X. Lu, L. Yu, Adsorption properties and mechanism of zinc acrylic carbon nanosphere aggregates for perfluorooctanoic acid from aqueous solution, Environ. Pollut., 316 (2023) 120540, doi: 10.1016/j.envpol.2022.120540.
[52] Ch. J. Mate, S. Mishra, Synthesis of borax cross-linked Jhingan gum hydrogel for remediation of Remazol Brilliant Blue R (RBBR) dye from water: adsorption isotherm, kinetic, thermodynamic and biodegradation studies, Int. J. Biol. Macromol., 151 (2020) 677–690.
[53] Y. He, L. Zhang, X. An, G. Wan, W. Zhu, Y. Luo, Enhanced fluoride removal from water by rare earth (La and Ce) modified alumina: adsorption isotherms, kinetics, thermodynamics and mechanism, Sci. Total Environ., 688 (2019) 184–198.
[54] H.A. Ahmad, S.S. Ahmed, O. Amiri, Simple synthesis of $CeFeO_3$ nanostructures as an efficient visible-light-driven photocatalyst in degradation of Congo red dye: mechanism investigation, Int. J. Hydrogen Energy, 48 (2023) 3878–3892.
[55] D. Wang, Q. Zhu, Y. Su, J. Li, A. Wang, Z. Xing, Preparation of MgAlFe-LDHs as a deicer corrosion inhibitor to reduce corrosion of chloride ions in deicing salts, Ecotoxicol. Environ. Saf., 174 (2019) 164–174.
[56] A.E. Nemr, O. Abdelwahab, A. El-Sikaily, A. Khaled, Removal of direct blue-86 from aqueous solution by new activated carbon developed from orange peel, J. Hazard. Mater., 161 (2009) 102–110.
[57] Z. Manaa, D. Chebli, A. Bouguettoucha, H. Atout, A. Amrane, Low-cost photo-Fenton-like process for the removal of synthetic dye in aqueous solution at circumneutral pH, Arabian J. Sci. Eng., 44 (2019) 9859–9867.